Environmental Science & Technology Letters

Letter

pubs.acs.org/journal/estlcu

Interaction of Graphene Oxide with Bacterial Cell Membranes: Insights from Force Spectroscopy

Santiago Romero-Vargas Castrillón,*[,†,‡,§] François Perreault,[†,§] Andreia Fonseca de Faria,[†] and Menachem Elimelech[†]

[†]Department of Chemical and Environmental Engineering, Yale University, New Haven, Connecticut 06520-8286, United States

[‡]Department of Civil, Environmental, and Geo- Engineering, University of Minnesota, Minneapolis, Minnesota 55455-0116, United States

Supporting Information

ABSTRACT: Understanding the interactions of graphene oxide (GO) with biological membranes is crucial for the evaluation of GO's health and environmental impacts, its bactericidal activity, and to advance graphene-based biological and environmental applications. In an effort to understand graphene-induced bacterial inactivation, we studied the interaction of GO with bacterial (*Escherichia coli*) cell membranes using atomic force microscopy (AFM). Toward this goal, we devised a polydopamine-assisted experimental protocol to functionalize an AFM probe with GO nanosheets, and used AFM-based force spectroscopy to measure cell membrane−GO interaction forces. Our results show that GO−cell interactions are predominantly repulsive, with only sporadic adhesion forces being measured upon probe pull-off, which we attribute to lipopolysaccharide bridging. We provide evidence of the acellular oxidation of glutathione by GO, underscoring the role of oxidative pathways in GO-mediated bacterial cell inactivation. Our force spectroscopy results suggest that physicochemical interactions do not underlie the primary mode of action of GO in bacteria.

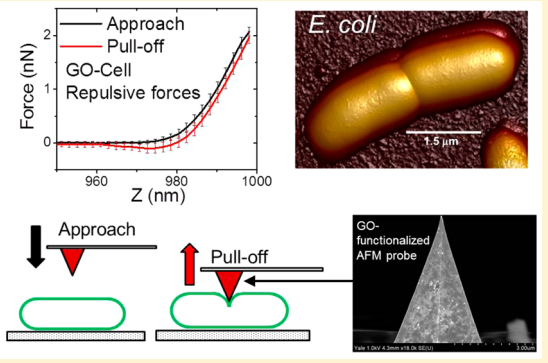

INTRODUCTION

Graphene is a monolayer-thick nanomaterial composed of hexagonally arranged carbon atoms. Since its first isolation from graphite in 2004, graphene has become the focus of numerous studies due to its unique physical properties, notably its mechanical strength[1] and electrical conductivity.[2] A common, low-cost preparation procedure of graphene materials involves the chemical reduction of graphene oxide (GO), with the latter being produced by oxidation of bulk graphite in the presence of strong oxidants.[3,4]

Interest in GO arises not only from its role as an inexpensive precursor of graphene, but also due to its distinct physicochemical properties. GO possesses hydrophilic functional groups (epoxide and hydroxyl groups on the surface and carboxylates at the periphery) as well as hydrophobic graphenic regions that enable it to engage in hydrophobic interactions while remaining dispersed in water and polar solvents.[5,6] In addition, owing to its nanoscale thickness, GO possesses a higher specific surface area than most other nanomaterials, enabling it to be used as an adsorbent or catalyst.[5] The amphiphilic character of GO has resulted in potential biomedical applications, such as a delivery device for small water-insoluble drugs.[5]

Recent studies have shown that GO and reduced GO exhibit toxicity toward both Gram-positive (*Staphylococcus aureus*) and Gram-negative (*Escherichia coli*) bacteria.[7,8] This property of GO can be used to fabricate antibacterial and biofilm-resistant surfaces, such as membranes for water purification,[9] polymeric films for biomedical devices,[10,11] and antimicrobial fabric materials.[12] GO-based membranes for water purification have also been reported recently.[13−15] Although the applications of GO are numerous, potential adverse health and environmental effects may also occur from cell exposure.[5,16,17] GO is both soluble in water and falls under the range of respirable materials.[18] Consequently, exposure to GO and its interaction with living organisms are likely to become a major concern. Yet, there is currently little, and often contradictory, information about the toxicity of GO and graphene-like nanomaterials.[19] In particular, a molecular level understanding of cell membrane−GO interactions leading to cell uptake or cell damage is lacking.[5]

A recent study combining molecular dynamics simulations with fluorescence and electron imaging techniques[18] reported that cell uptake of graphene occurs spontaneously in three different mammalian cell types, and is driven by spontaneous piercing of the membrane by nanosheet asperities, followed by hydrophobic interactions between the basal regions of graphene and the hydrophobic inner region of the plasma membrane. Another experimental-computational study[20] suggested that graphene and GO induce cell damage in *E. coli* by extracting

Received: January 25, 2015
Accepted: March 25, 2015
Published: March 25, 2015

DOI: 10.1021/acs.estlett.5b00066
Environ. Sci. Technol. Lett. 2015, 2, 112−117

phospholipid molecules from the outer cell membrane. Oxidative stress has also been invoked to explain GO-induced cell damage,[17] either by generation of reactive oxygen species (e.g., the superoxide anion, $O_2^{\cdot -}$),[21] or through direct oxidation of cellular components by GO.[22]

In this study, we examine the physicochemical interactions of GO with bacterial cells. Specifically, we measure the interaction forces between a probe functionalized with GO and model Gram-negative bacteria (*E. coli*) using atomic force microscopy (AFM). We report a method to functionalize AFM probes with GO, which, together with immobilization of *E. coli* cells on a surface, allows for cell−GO forces to be measured. We find that the interaction forces between a GO-functionalized AFM probe and the outer cell membrane of *E. coli* are mainly repulsive, with only sporadic adhesive forces being observed in the pull-off force curves. We discuss our findings in the context of bacterial cytotoxicity of GO.

MATERIALS AND METHODS

Fabrication of Bacterial Lawns. *Escherichia coli* (strain MV1190(*λ-pir*)(pJBA116)) cells were immobilized on glass slides coated with poly-L-lysine (MW = 150−300 kDa), adapting a protocol from the literature.[23] Cell suspensions were prepared by inoculating 25 mL of Luria-Bertani (LB) broth with cell colonies grown on agar plates, and incubated overnight at 37 °C. The cell suspension was diluted 1:25 with fresh LB, and cells in exponential growth phase ($OD_{600\ nm} \approx 1$, 10^9 cells/mL) were harvested after further incubation for 2 h at 37 °C, centrifuged to a pellet at 5000*g* for 1 min, and resuspended in PBS buffer (pH 7.4, 1:5 dilution). Cell centrifugation and resuspension was repeated thrice, with the final cell resuspension being done in diluted PBS supplemented with 1 mg/mL 1-ethyl-3-(3-dimethylaminopropyl)carbodiimide (EDC, Thermo Scientific) and 2 mg/mL *N*-hydroxysuccinimide (NHS, Sigma-Aldrich). Activation for 15 min with EDC and NHS converts the carboxylic groups on the cell surface into amine-reactive succinimidyl esters.[23,24] Finally, a 10 μL drop of the cell suspension with EDC−NHS was placed on a small (∼1 cm^2) glass slide coupon coated with poly-L-lysine (PLL) (Poly-prep, Sigma-Aldrich). Cells are immobilized on the surface by an amine-coupling reaction between the succinimidyl esters on the outer cell membrane and primary amines on the PLL coating the glass slide. We imaged the immobilized cells by AFM, and assessed their viability by epifluorescence microscopy, as explained in the Supporting Information.

AFM Probe Functionalization with Graphene Oxide. We produced GO following a modified Hummers' method.[25] The average GO sheet surface area and thickness were measured by scanning electron microscopy (SEM) and tapping-mode AFM, and determined to be 0.65 μm^2 and 1.4 nm, respectively (Figure S1, Supporting Information). XPS characterization (Figure S2, Supporting Information) showed the presence of hydroxyl, epoxide and carboxyl functional groups in GO nanosheets. Details of the GO synthesis and characterization can be found in the Supporting Information.

Force measurements were carried out using silicon nitride cantilevers (SNL, Bruker, nominal k = 0.24 N/m) that were functionalized with GO, as described in Figure 1. The surface functionalization is assisted by the deposition of polydopamine on the AFM probe. Under slightly alkaline conditions, dopamine forms a supramolecular aggregate known as polydopamine (PDA)[26,27] on the AFM probe surface that serves as a scaffold for the adsorption of GO nanosheets. A

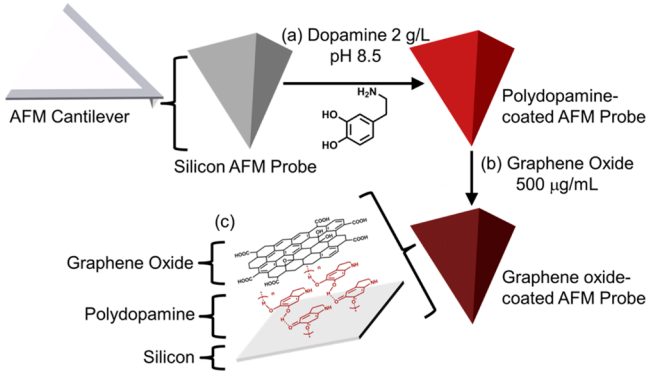

Figure 1. Schematic of the AFM probe functionalization with graphene oxide. (a) Immersion of the AFM cantilever in an aqueous solution of dopamine results in deposition of a thin adherent film of polydopamine on the probe surface. (b) Subsequent immersion in an aqueous dispersion of graphene oxide results in immobilization of the nanomaterial on the probe surface. The components of the functionalized probe surface are depicted in (c), where polydopamine is described as a supramolecular aggregate of dopamine monomers, as recently proposed.[27]

PDA film was formed on the AFM probe by immersing the probe in a solution containing 2 mg/mL of dopamine hydrochloride (Sigma-Aldrich) in 10 mM Tris (Trizma HCl, Sigma-Aldrich), pH 8.5. Over the course of the immersion the solution turned brown due to aggregation of dopamine monomers. After immersion in PDA solution for 15 min under agitation, the cantilever was rinsed with deionized water and transferred to a dispersion of GO (500 μg/mL) for 15 min, followed by rinsing with deionized water to removed loosely adsorbed sheets. Cantilevers were dried at room temperature under vacuum until use.

In addition to measurements performed with GO-functionalized probes (PDA-GO, hereinafter), we performed control experiments using PDA-coated and unmodified silicon cantilevers (hereinafter PDA and Si, respectively). All cantilevers were cleaned in a UV/ozone chamber before modification. All AFM probes were imaged by SEM after the experiments and inspected for defects, cracks, or evidence of contamination.

AFM Force Measurements. Previous studies have shown the versatility of AFM in examining the mechanical properties of cells exposed to carbon-based nanomaterials.[28,29] In this work, we determine GO−cell membrane forces using AFM. Force measurements were made in PBS buffer (1:5 dilution), pH 7.4, using a Dimension Icon AFM (Bruker). Prior to the force measurements we determined the cantilever deflection sensitivity and calibrated the spring constant using the thermal noise method. We observed in preliminary experiments that imaging the bacterial lawn to identify cells for force measurements resulted in functionalized probe damage or contamination. To circumvent AFM imaging, we used the indentation of soft materials (such as *E. coli*) to identify measurements performed on cell membranes from those made on the bare PLL slide. The indentation is defined as the separation (in nm) between the onset of the compliance region (i.e., the point at which the approach force becomes finite due to tip−sample contact) and the maximum force in the approach curve. As shown below, force curves with an indentation >20 nm denoted measurements on individual cells, whereas those exhibiting a smaller indentation were measured on the PLL coating (which were not considered further in this work). At

DOI: 10.1021/acs.estlett.5b00066
Environ. Sci. Technol. Lett. 2015, 2, 112−117

least 10 cell-probe force measurements (ramp size = 1 μm, trigger force = 2 nN) were performed with Si, PDA and PDA-GO probes. Further information about our force spectroscopy experimental protocol may be found in the Supporting Information.

Quantification of GO-Mediated Oxidative Stress. Reduced glutathione (0.4 mM) was exposed to GO (50 μg/mL) in 50 mM bicarbonate buffer (pH 8.6). The amount of nonoxidized glutathione was quantified spectrophotometrically using Ellman's reagent, 5,5′-dithiobis(2-nitrobenzoic acid) (DTNB). After exposure to GO for 0–240 min, the reaction mixture was filtered through a 0.45 μm filter to remove GO sheets and 900 μL of the filtered reaction mixture were added to 1.57 mL Tris–HCl buffer (pH 8.3) to which 30 μL of 100 mM DTNB was added. The amount of thiol remaining in the reaction was quantified by measuring the absorbance at 412 nm, using an extinction coefficient of 14 150 M^{-1} cm^{-1}.

RESULTS AND DISCUSSION

Cell Immobilization and AFM Imaging. Immobilization of cells without significant alteration in their morphology and surface properties is essential in force spectroscopy. We adapted a protocol from the literature[23] to form bacterial cell lawns suitable for cell–probe force measurements. An AFM image of a representative bacterial cell lawn is shown in Figure 2a. The cell dimensions (~1 × ~3 μm) are in agreement with the size of *E. coli*.[30,31] *E. coli* cells are immobilized on a PLL-coated glass slide by amine coupling. The immobilization is also assisted by electrostatic interactions between the negatively charged *E. coli* and the positively charged PLL surface. We performed the immobilization and experiments in PBS buffer at 1:5 dilution to diminish charge screening and prevent cell–cell aggregation. We verified that the immobilization protocol does not significantly affect the cell viability. Figure 2c shows an epifluorescence micrograph of the cells after Live/Dead staining. As shown in Figure 2b, approximately 80% of the cells remain viable (i.e., exhibit green fluorescence) following immobilization. We note that the EDC–NHS immobilization does not alter the surface properties of the cell membrane exposed to the AFM probe, given that succinimidyl esters have a half-life on the order of minutes at pH 7.4.[24,32–34]

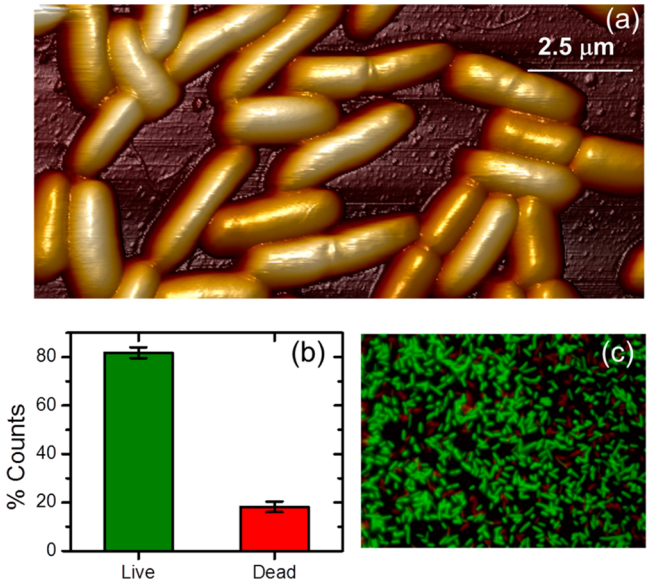

Figure 2. (a) AFM image of *E. coli* cells immobilized on a poly-L-lysine-coated glass slide. Cells were covalently immobilized by a coupling reaction between the carboxyl groups on the cell membrane surface and amine groups on the substrate surface. The image shown was obtained in peak force tapping mode at a scan rate of 1 Hz. All experiments were performed in PBS buffer (1:5 dilution), pH 7.4. (b) Results of a live–dead assay on representative immobilized cells. Approximately 80% of the immobilized cells had intact cell membranes following the immobilization, and therefore fluoresced green as shown in (c). Cells with a compromised cell membrane fluoresced red.

Polydopamine Enables Probe Functionalization with GO. Figures 3 and S3 (Supporting Information) present SEM micrographs of Si, PDA, and PDA-GO AFM probes. In each case, the surface of the pyramidal probes exhibits distinct features: the Si probe surface (Figures 3c and S3d, Supporting Information) is smooth and featureless, whereas the PDA-coated tip (Figures 3b and S3c, Supporting Information) shows the presence of PDA agglomerates. Unlike the Si and PDA systems, the surface of the PDA-GO probe shows the presence of GO sheets, as manifested by the tile-like dark features in Figures 3a and S3a, Supporting Information, and rougher surface features in Figure S3b (Supporting Information). Attachment of GO sheets to the polydopamine-coated surface is due to hydrogen bond interactions between carbonyl and hydroxyl groups abundant in both PDA and GO, and π–π interactions between catechol groups in PDA and graphenic domains in GO.[35]

We verified that the self-adherent film of PDA is necessary for the functionalization: in its absence GO does not adhere to the probe Si surface (Figure S3d, Supporting Information). We surmise that, in addition to favorable interactions for GO attachment, the PDA film screens the electrostatic repulsive forces between negatively charged GO (electrophoretic mobility of $-4.11 \pm 0.29 \times 10^{-8}$ m^2 V^{-1} s^{-1} in PBS 1:5 dilution) and deprotonated silanol groups on the probe surface.[36,37] To provide further evidence of the validity of the functionalization method, we subjected a silicon wafer to the GO protocol illustrated in Figure 1. We tested the robustness of the functionalization by immersing the PDA-GO wafer in PBS buffer (1:5 dilution, pH 7.4) for 1 h, the typical duration of AFM measurements. We then recorded the Raman spectra (Horiba Jobin Yvon HR-800) of vacuum-dried samples. Figure 3d shows that the Raman spectrum of the PDA-GO wafer exhibits the D (~1350 cm^{-1}) and G (~1590 cm^{-1}) bands characteristic of GO.[38] Conversely, the spectra of PDA-coated and pristine Si wafers do not exhibit such features.

Cell–GO Interactions are Predominantly Repulsive. Figure 4 presents force curves measured on individual cells with probes of various chemistries (Si, PDA, and PDA-GO). The average of 10–14 individual force curves is shown. The individual force curve measurements made with each probe chemistry are shown in Figure S4a–f of the Supporting Information. Each curve comprises approach (Figure 4a, b) and pull-off (Figure 4c, d) cycles. The data are presented as plots of the force as a function of piezo position (Z). We identified forces on cells from those measured on the PLL slide by measuring the indentation in the approach force curve. In a series of measurements with a pristine Si probe, we imaged individual cells before measuring the force curves using the "Point and Shoot" function implemented in the AFM software (NanoScope, Bruker, Santa Barbara). We determined the indentation on the cells to be 20–25 nm, as shown in Figure 4a. Meanwhile, the indentation on bare PLL was ~10 nm

DOI: 10.1021/acs.estlett.5b00066
Environ. Sci. Technol. Lett. 2015, 2, 112–117

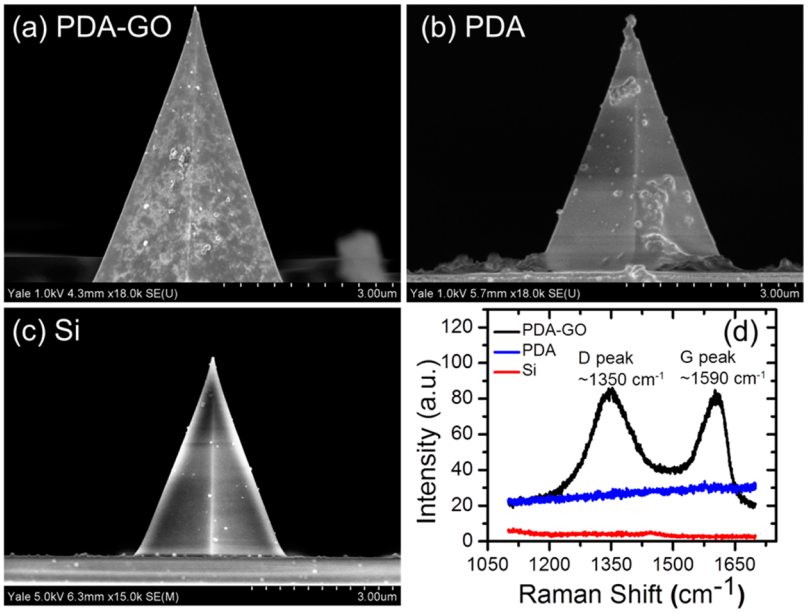

Figure 3. (a) Scanning electron micrograph (SEM) of an AFM probe functionalized with graphene oxide (PDA-GO), following the protocol in Figure 1. (b) SEM micrographs of polydopamine-coated (PDA) and pristine Si (c) AFM probes. The imaged samples in panels a–c were not sputter-coated. (d) Raman spectrum of a Si wafer functionalized with graphene oxide (PDA-GO, black line), as described in Figure 1. The spectrum shows the characteristic D and G bands of GO. The Raman spectra of pristine and PDA-coated Si wafers are also shown.

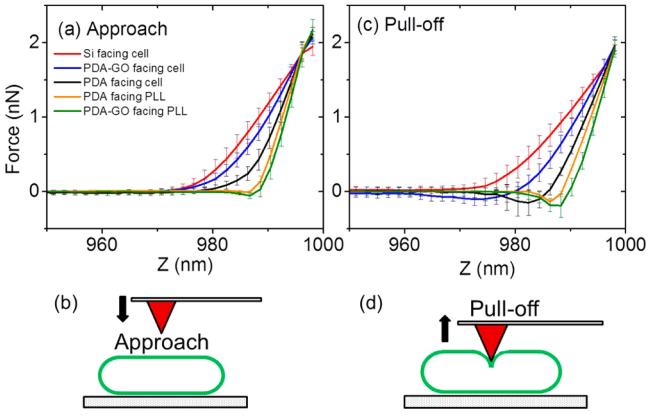

Figure 4. Plots of the force as a function of piezo position (Z) during cantilever approach to (a, b) and pull-off from (c, d) *E. coli* cells. The AFM probe functionalization is denoted in the caption of (a), indicating whether measurements are made on cells ("facing cell") or the bare PLL-coated glass slide ("facing PLL"). Each curve is the average of 10 independent force measurements (14 measurements for PDA-GO). Error bars denote one standard deviation in the force.

(Figure 4a). Details of the definition and determination of the indentation are given in the Materials and Methods section.

A key observation in Figure 4a is that the approach force curves for the Si and PDA-GO probes are both repulsive and within one standard deviation of each other. This observation is reproducible over all the measurements performed in 2–4 different cells (Figure S4a, c, Supporting Information). Repulsive Si–cell interactions have been previously observed,[39] and are attributed to the negatively charged surface of the silicon probe (due to the presence of deprotonated silanol groups[36]) and the outer cell membrane of *E. coli*.[39,40] We surmise that the repulsive GO–cell forces in Figure 4a arise from electrostatic repulsion between deprotonated carboxylic acid groups in GO[37,41] and the negatively charged outer cell membrane. Given the presence of lipopolysaccharide molecules on the cell surface, steric repulsion is also a likely contributor to the observed repulsive forces.[42,43] Repulsive PDA–cell forces are also observed in the PDA control measurements in Figure 4a, possibly due to the reported negative surface charge of PDA films[44] as well as steric forces. PDA–cell repulsive interactions are somewhat weaker compared to those measured with Si and PDA–GO probes. Finally, we note that interaction force curves characteristic of cell membrane piercing events[45] were not observed in any of our experiments.

The repulsive forces characterizing GO–cell contact are at odds with certain aspects of recent computational-experimental studies,[18,20] which suggest that physical–chemical interactions between graphene/GO and cells result in membrane damage. To explain the discrepancy between our experimental results and previous works,[18,20] we first note that simulation studies have noted the strong influence of the relative orientations of graphene and the cell on the free energy of interaction.[18] Graphene sheets that point an asperity orthogonally to the cell membrane appear to face the smallest free energy barrier.[18,20] Our experimental results are consistent with the strong directionality of GO–cell interactions, because GO sheets immobilized on the AFM probe are locked into a fixed configuration, precluding sampling of more energetically favorable pathways for membrane piercing. Second, simulation results have noted that model GO sheets with hydrophilic corners do not undergo cell uptake.[18] This picture is consistent with the repulsive forces between hydrophilic GO (owing to carboxylic, hydroxyl, and epoxide functional groups of GO,[41] Figure S2, Supporting Information) and cells reported herein.

The average pull-off force curves are presented in Figure 4c. The averaged data show weak adhesions for PDA ($F_{adhesion,min} \approx -0.15$ nN) and PDA-GO ($F_{adhesion,min} \approx -0.10$ nN). The individual measurements are shown in Figure S4b, d, f of the Supporting Information. While the pull-off force curves measured with the Si probe are predominantly repulsive (Figure S4b, Supporting Information), those corresponding to PDA-GO and PDA (Figure S4d, f, respectively, Supporting

DOI: 10.1021/acs.estlett.5b00066
Environ. Sci. Technol. Lett. 2015, 2, 112–117

Information), show evidence of adhesion. For PDA-GO (Figure S4d, Supporting Information), the adhesion events are similar to those derived from the extension of polymer molecules between the cell surface and the AFM tip.[42,46,47] We suggest that lipopolysaccharides in the *E. coli* surface become stretched as they bridge the cell surface and the GO-coated AFM tip. Finally, electrostatic interactions between positively charged bare PLL surfaces and the negatively charged functionalized probes manifest themselves in slightly stronger adhesion forces for PDA facing PLL (−0.14 nN) and PDA-GO on PLL (−0.19 nN), as shown in Figure 4c.

Implications for the Bactericidal Activity of GO. Bacterial inactivation by GO has been proposed to be mediated by physical and oxidative damage to cell membranes.[22] Physical interactions underlying the antimicrobial activity of GO include membrane piercing, surface adhesion, and lipid extraction.[18−20] Our results show that direct contact between GO and the outer cell membrane of *E. coli* is characterized by repulsive interactions, with only sporadic adhesion events observed upon probe pull-off, likely due to cell lipopolysaccharide bridging. These results are consistent with the high free energy barrier for cell uptake faced by hydrophilic GO sheets.[18]

Recent studies have indicated that direct contact with the edges of the GO sheets is not a requirement for bacterial inactivation,[48,49] suggesting that other mechanisms may play a predominant role in the bactericidal activity of GO. Oxidative stress, in particular, has been identified as an antimicrobial mechanism for carbon nanomaterials,[50,51] including GO.[52,53]

GO is inherently chemically reactive, as indicated by the acellular oxidation of glutathione by GO sheets (Figure S5, Supporting Information). This in vitro oxidation of glutathione was previously used as an indicator of the oxidative potential of carbon nanotubes,[50,54] where oxidative stress was proposed as the major mechanism underlying antimicrobial activity.[50,51,54] For GO, further investigations are needed to unravel the exact contribution of oxidative and physical pathways in the antimicrobial activity of GO. A mechanism for the bactericidal activity of GO based on physicochemical interactions is intuitively appealing and cannot be ruled out at this point. Nonetheless, the force spectroscopy results presented herein suggest that physical interactions are repulsive and that other mechanisms, such as oxidative pathways, should be examined more closely.

■ ASSOCIATED CONTENT

Supporting Information

Additional materials and methods information (cell imaging, GO synthesis and characterization, force spectroscopy); GO characterization (Figures S1 and S2), additional AFM cantilever SEM imaging (Figure S3); complete approach and pull-off force curve data (Figure S4); in vitro glutathione oxidation assay results (Figure S5). This material is available free of charge via the Internet at http://pubs.acs.org.

■ AUTHOR INFORMATION

Corresponding Author

*S. Romero-Vargas Castrillón. E-mail: sromerov@umn.edu. Tel: +1 612 301 1347. Fax: +1 612 626 7750.

Author Contributions

§S.R.-V.C. and F.P. were equal contributors to this work.

Notes

The authors declare no competing financial interest.

■ ACKNOWLEDGMENTS

We acknowledge the NSERC Postdoctoral Fellowship awarded to F.P. A.F.F. acknowledges the financial support of the Science without Borders program through the Brazilian Council of Science and Technology (CNPq Grant 246407/2012-3), and the Lemann Institute for Brazilian Studies. Facilities use was supported by YINQE and NSF MRSEC DMR 1119826. We thank Dr. Siamak Nejati for assistance with SEM and XPS analysis. We also thank Dr. Kanani Lee for granting access to the Raman spectrometer and Dr. George Amulele for his technical assistance.

■ REFERENCES

(1) Lee, C.; Wei, X. D.; Kysar, J. W.; Hone, J. Measurement of the elastic properties and intrinsic strength of monolayer graphene. *Science* **2008**, *321*, 385−388.

(2) Geim, A. K.; Novoselov, K. S. The rise of graphene. *Nat. Mater.* **2007**, *6*, 183−191.

(3) Roy-Mayhew, J. D.; Aksay, I. A. Graphene materials and their use in dye-sensitized solar cells. *Chem. Rev.* **2014**, *114*, 6323−6348.

(4) Gao, W.; Alemany, L. B.; Ci, L. J.; Ajayan, P. M. New insights into the structure and reduction of graphite oxide. *Nat. Chem.* **2009**, *1*, 403−408.

(5) Sanchez, V. C.; Jachak, A.; Hurt, R. H.; Kane, A. B. Biological interactions of graphene-family nanomaterials: An interdisciplinary review. *Chem. Res. Toxicol.* **2012**, *25*, 15−34.

(6) Paredes, J. I.; Villar-Rodil, S.; Martinez-Alonso, A.; Tascon, J. M. D. Graphene oxide dispersions in organic solvents. *Langmuir* **2008**, *24*, 10560−10564.

(7) Akhavan, O.; Ghaderi, E. Toxicity of graphene and graphene oxide nanowalls against bacteria. *ACS Nano* **2010**, *4*, 5731−5736.

(8) Hu, W. B.; Peng, C.; Luo, W. J.; Lv, M.; Li, X. M.; Li, D.; Huang, Q.; Fan, C. H. Graphene-based antibacterial paper. *ACS Nano* **2010**, *4*, 4317−4323.

(9) Perreault, F.; Tousley, M. E.; Elimelech, M. Thin-film composite polyamide membranes functionalized with biocidal graphene oxide nanosheets. *Environ. Sci. Technol. Lett.* **2014**, *1*, 71−76.

(10) Carpio, I. E. M.; Santos, C. M.; Wei, X.; Rodrigues, D. F. Toxicity of a polymer-graphene oxide composite against bacterial planktonic cells, biofilms, and mammalian cells. *Nanoscale* **2012**, *4*, 4746−4756.

(11) Mazaheri, M.; Akhavan, O.; Simchi, A. Flexible bactericidal graphene oxide-chitosan layers for stem cell proliferation. *Appl. Surf. Sci.* **2014**, *301*, 456−462.

(12) Karimi, L.; Yazdanshenas, M. E.; Khajavi, R.; Rashidi, A.; Mirjalili, M. Using graphene/TiO_2 nanocomposite as a new route for preparation of electroconductive, self-cleaning, antibacterial and antifungal cotton fabric without toxicity. *Cellulose* **2014**, *21*, 3813−3827.

(13) Mi, B. X. Graphene oxide membranes for ionic and molecular sieving. *Science* **2014**, *343*, 740−742.

(14) Hu, M.; Mi, B. X. Layer-by-layer assembly of graphene oxide membranes via electrostatic interaction. *J. Membr. Sci.* **2014**, *469*, 80−87.

(15) Joshi, R. K.; Carbone, P.; Wang, F. C.; Kravets, V. G.; Su, Y.; Grigorieva, I. V.; Wu, H. A.; Geim, A. K.; Nair, R. R. Precise and ultrafast molecular sieving through graphene oxide membranes. *Science* **2014**, *343*, 752−754.

(16) Zhao, J.; Wang, Z. Y.; White, J. C.; Xing, B. S. Graphene in the aquatic environment: adsorption, dispersion, toxicity and transformation. *Environ. Sci. Technol.* **2014**, *48*, 9995−10009.

(17) Seabra, A. B.; Paula, A. J.; de Lima, R.; Alves, O. L.; Duran, N. Nanotoxicity of graphene and graphene oxide. *Chem. Res. Toxicol.* **2014**, *27*, 159−168.

(18) Li, Y. F.; Yuan, H. Y.; von dem Bussche, A.; Creighton, M.; Hurt, R. H.; Kane, A. B.; Gao, H. J. Graphene microsheets enter cells

DOI: 10.1021/acs.estlett.5b00066
Environ. Sci. Technol. Lett. 2015, 2, 112−117

through spontaneous membrane penetration at edge asperities and corner sites. *Proc. Natl. Acad. Sci. U. S. A.* **2013**, *110*, 12295−12300.
(19) Kostarelos, K.; Novoselov, K. S. Exploring the interface of graphene and biology. *Science* **2014**, *344*, 261−263.
(20) Tu, Y. S.; Lv, M.; Xiu, P.; Huynh, T.; Zhang, M.; Castelli, M.; Liu, Z. R.; Huang, Q.; Fan, C. H.; Fang, H. P.; Zhou, R. H. Destructive extraction of phospholipids from *Escherichia coli* membranes by graphene nanosheets. *Nat. Nanotechnol.* **2013**, *8*, 594−601.
(21) Zhang, Y. B.; Ali, S. F.; Dervishi, E.; Xu, Y.; Li, Z. R.; Casciano, D.; Biris, A. S. Cytotoxicity effects of graphene and single-wall carbon nanotubes in neural phaeochromocytoma-derived PC12 cells. *ACS Nano* **2010**, *4*, 3181−3186.
(22) Liu, S. B.; Zeng, T. H.; Hofmann, M.; Burcombe, E.; Wei, J.; Jiang, R. R.; Kong, J.; Chen, Y. Antibacterial activity of graphite, graphite oxide, graphene oxide, and reduced graphene oxide: Membrane and oxidative stress. *ACS Nano* **2011**, *5*, 6971−6980.
(23) Meyer, R. L.; Zhou, X. F.; Tang, L. N.; Arpanaei, A.; Kingshott, P.; Besenbacher, F. Immobilisation of living bacteria for AFM imaging under physiological conditions. *Ultramicroscopy* **2010**, *110*, 1349−1357.
(24) Grabarek, Z.; Gergely, J. Zero-length crosslinking procedure with the use of active esters. *Anal. Biochem.* **1990**, *185*, 131−135.
(25) Tung, V. C.; Allen, M. J.; Yang, Y.; Kaner, R. B. High-throughput solution processing of large-scale graphene. *Nat. Nanotechnol.* **2009**, *4*, 25−29.
(26) Lee, H.; Dellatore, S. M.; Miller, W. M.; Messersmith, P. B. Mussel-inspired surface chemistry for multifunctional coatings. *Science* **2007**, *318*, 426−430.
(27) Dreyer, D. R.; Miller, D. J.; Freeman, B. D.; Paul, D. R.; Bielawski, C. W. Elucidating the structure of poly(dopamine). *Langmuir* **2012**, *28*, 6428−6435.
(28) Liu, S. B.; Wei, L.; Hao, L.; Fang, N.; Chang, M. W.; Xu, R.; Yang, Y. H.; Chen, Y. Sharper and faster "nano darts" kill more bacteria: A study of antibacterial activity of individually dispersed pristine single-walled carbon nanotube. *ACS Nano* **2009**, *3*, 3891−3902.
(29) Liu, S. B.; Ng, A. K.; Xu, R.; Wei, J.; Tan, C. M.; Yang, Y. H.; Chen, Y. A. Antibacterial action of dispersed single-walled carbon nanotubes on *Escherichia coli* and *Bacillus subtilis* investigated by atomic force microscopy. *Nanoscale* **2010**, *2*, 2744−2750.
(30) Nelson, D. E.; Young, K. D. Penicillin binding protein 5 affects cell diameter, contour, and morphology of *Escherichia coli*. *J. Bacteriol.* **2000**, *182*, 1714−1721.
(31) Grossman, N.; Ron, E. Z.; Woldringh, C. L. Changes in cell dimensions during amino-acid starvation of *Escherichia coli*. *J. Bacteriol.* **1982**, *152*, 35−41.
(32) Thelen, P.; Deuticke, B. Chemo-mechanical leak formation in human-erythrocytes upon exposure to a water-soluble carbodiimide followed by very mild shear-stress 0.2. Chemical modifications involved. *Biochim. Biophys. Acta* **1988**, *944*, 297−307.
(33) Cuatrecasas, P.; Parikh, I. Adsorbents for affinity chromatography. Use of N-hydroxysuccinimide esters of agarose. *Biochemistry* **1972**, *11*, 2291−2299.
(34) Schasfoort, R. B. M.; Tudos, A. J. *Handbook of Surface Plasmon Resonance*; RSC Pub.: Cambridge, U. K., 2008.
(35) Hwang, S. H.; Kang, D.; Ruoff, R. S.; Shin, H. S.; Park, Y. B. Poly(vinyl alcohol) reinforced and toughened with poly(dopamine)-treated graphene oxide, and its use for humidity sensing. *ACS Nano* **2014**, *8*, 6739−6747.
(36) Butt, H. J.; Jaschke, M.; Ducker, W. Measuring surface forces in aqueous-electrolyte solution with the atomic-force microscope. *Bioelectrochem. Bioenerg.* **1995**, *38*, 191−201.
(37) Li, D.; Muller, M. B.; Gilje, S.; Kaner, R. B.; Wallace, G. G. Processable aqueous dispersions of graphene nanosheets. *Nat. Nanotechnol.* **2008**, *3*, 101−105.
(38) Kudin, K. N.; Ozbas, B.; Schniepp, H. C.; Prud'homme, R. K.; Aksay, I. A.; Car, R. Raman spectra of graphite oxide and functionalized graphene sheets. *Nano Lett.* **2008**, *8*, 36−41.
(39) Razatos, A.; Ong, Y. L.; Sharma, M. M.; Georgiou, G. Molecular determinants of bacterial adhesion monitored by atomic force microscopy. *Proc. Natl. Acad. Sci. U. S. A.* **1998**, *95*, 11059−11064.
(40) Walker, S. L.; Hill, J. E.; Redman, J. A.; Elimelech, M. Influence of growth phase on adhesion kinetics of *Escherichia coli* D21g. *Appl. Environ. Microbiol.* **2005**, *71*, 3093−3099.
(41) Dreyer, D. R.; Todd, A. D.; Bielawski, C. W. Harnessing the chemistry of graphene oxide. *Chem. Soc. Rev.* **2014**, *43*, 5288−5301.
(42) Camesano, T. A.; Logan, B. E. Probing bacterial electrosteric interactions using atomic force microscopy. *Environ. Sci. Technol.* **2000**, *34*, 3354−3362.
(43) de Kerchove, A. J.; Elimelech, M. Relevance of electrokinetic theory for "soft" particles to bacterial cells: Implications for bacterial adhesion. *Langmuir* **2005**, *21*, 6462−6472.
(44) Liu, Q. Z.; Yu, B.; Ye, W. C.; Zhou, F. Highly selective uptake and release of charged molecules by pH-responsive polydopamine microcapsules. *Macromol. Biosci.* **2011**, *11*, 1227−1234.
(45) Goncalves, R. P.; Agnus, G.; Sens, P.; Houssin, C.; Bartenlian, B.; Scheuring, S. Two-chamber AFM: Probing membrane proteins separating two aqueous compartments. *Nat. Methods* **2006**, *3*, 1007−1012.
(46) Heinz, W. F.; Hoh, J. H. Spatially resolved force spectroscopy of biological surfaces using the atomic force microscope. *Trends Biotechnol.* **1999**, *17*, 143−150.
(47) Ong, Y. L.; Razatos, A.; Georgiou, G.; Sharma, M. M. Adhesion forces between *E. coli* bacteria and biomaterial surfaces. *Langmuir* **1999**, *15*, 2719−2725.
(48) Hui, L. W.; Piao, J. G.; Auletta, J.; Hu, K.; Zhu, Y. W.; Meyer, T.; Liu, H. T.; Yang, L. H. Availability of the basal planes of graphene oxide determines whether it is antibacterial. *ACS Appl. Mater. Interfaces* **2014**, *6*, 13183−13190.
(49) Mangadlao, J. D.; Santos, C. M.; Felipe, M. J. L.; de Leon, A. C. C.; Rodrigues, D. F.; Advincula, R. C. On the antibacterial mechanism of graphene oxide (GO) Langmuir−Blodgett films. *Chem. Commun.* **2015**, *51*, 2886−2889.
(50) Vecitis, C. D.; Zodrow, K. R.; Kang, S.; Elimelech, M. Electronic-structure-dependent bacterial cytotoxicity of single-walled carbon nanotubes. *ACS Nano* **2010**, *4*, 5471−5479.
(51) Kang, S.; Herzberg, M.; Rodrigues, D. F.; Elimelech, M. Antibacterial effects of carbon nanotubes: Size does matter. *Langmuir* **2008**, *24*, 6409−6413.
(52) Gurunathan, S.; Han, J. W.; Dayem, A. A.; Eppakayala, V.; Kim, J. H. Oxidative stress-mediated antibacterial activity of graphene oxide and reduced graphene oxide in *Pseudomonas aeruginosa*. *Int. J. Nanomed.* **2012**, *7*, 5901−5914.
(53) Chen, J. N.; Wang, X. P.; Han, H. Y. A new function of graphene oxide emerges: Inactivating phytopathogenic bacterium *Xanthomonas oryzae pv. Oryzae*. *J. Nanopart. Res.* **2013**, *15*.
(54) Pasquini, L. M.; Sekol, R. C.; Taylor, A. D.; Pfefferle, L. D.; Zimmerman, J. B. Realizing comparable oxidative and cytotoxic potential of single-and multiwalled carbon nanotubes through annealing. *Environ. Sci. Technol.* **2013**, *47*, 8775−8783.

DOI: 10.1021/acs.estlett.5b00066
Environ. Sci. Technol. Lett. 2015, 2, 112−117